Defining the best strain gauge placement through numerical simulations of the mechanical behavior of the Modified-WOL specimen

Emerson T. Marcelino[1], Jorge A.P. Carrasco[1], José M.A. Barbosa[1], Nadège S. Bouchonneau[1]

[1]*Federal University of Pernambuco, Department of Mechanical Engineering, Av. da Arquitetura, s/n, Cidade Universitária, Recife – PE – Brazil, 50740-550.*
emerson.trindadem@ufpe.br, jorge.carrasco@ufpe.br, jose.mabarbosa@ufpe.br, nadege.bouchonneau@ufpe.br

Abstract. The occurrence of cracks in metallic structures is inevitable, which necessitates assessments of their resistance to crack propagation under various loads and environmental conditions. However, experimentally determining fracture parameters is costly and time-consuming, needing multiple specimens and extensive testing. An alternative is a test using the Modified-WOL specimen with a bolt for self-loading, aiming to provide the Threshold Stress Intensity Factor for Environment-Assisted Cracking with a single specimen. Electronic instrumentation is crucial for real-time data but lacks consensus on sensor placement, which may affect mechanical response. This study investigates the mechanical behavior of the Modified-WOL specimen components using the Finite Element Method with 3D models and the Augmented Lagrangian method. The results are consistent with empirical values, allowing us to identify and recommend the best location for strain gauge installation.

Keywords: Modified-WOL specimen, Finite Element Method, Augmented Lagrangian method.

1 Introduction

In structural steels, cracks are an inevitable occurrence as they can be introduced during manufacturing or in service, demanding an examination of their ability to resist crack propagation under expected loads and various environmental conditions. The combination of mechanical loads, environmental effects, and crack can cause local degradation, reducing the fracture toughness of the material and leading to structural failure. This delayed fracture process is known as Environmental Assisted Cracking (EAC) [1, 2].

Therefore, it is imperative to ensure that the stresses generated in the structures are insufficient to initiate EAC, or that the crack growth occurring during the design life or between inspection periods is tolerable without the risk of unstable fracture [3]. Considering the degradation that occurs in materials subjected to these environmental processes, the principles of Linear Elastic Fracture Mechanics (LEFM) can be used to quantify the stress in the region ahead of a crack tip in the structure or in a pre-cracked specimen in terms of the Stress Intensity Factor in Plane Strain for Mode I loading (K_I), thereby determining the Threshold Stress Intensity Factor for EAC in Mode I loading (K_{IEAC}).

However, the experimental determination of K_{IEAC} using constant load or constant displacement tests, currently used in laboratories, is costly due to the need for multiple specimens, sophisticated equipment and systems, and the involvement of specialized technicians. An alternative method is the constant displacement test conducted with the Modified Bolt-Load Compact Specimen, also known as the Modified-WOL specimen, which is currently standardized by ISO 7539-6 [3] and ASTM E1681-23ε1 [4].

The Modified-WOL specimen is equipped with a bolt and a reaction pin for self-loading, thus not requiring any tensile testing machine. This results in a compact and easy-to-use system that can be placed directly in the

environmental chamber where the aggressive effects of the working environment will be reproduced. The primary objective of this method is to provide K_{IEAC} utilizing only a single specimen [3, 5, 6]. The incorporation of electronic instrumentation is essential for obtaining reliable and real-time data.

Different instrumentation methods were identified for the initial loading phase of the Modified-WOL specimen. The most common technique was the use of a clip gauge, which measures the crack mouth opening displacement (CMOD) [7-12] to indirectly calculate the bolt load [3]. Ming *et al*. [13] used a dial gauge to measure the CMOD. Two studies combined the clip gauge with instrumentation of the reaction pin's lateral faces using strain gauges to monitor crack growth [7, 11]. Two articles used the Back Face Strain (BFS) technique, indirectly measuring the load applied by the bolt with strain gauges on the specimen's back face [14-15].

The second most common technique identified was the use of instrumented bolts to directly measure the applied load [16-20]. Chung, Cragnolino, and Macdonald [21] tested a compression load cell, an externally instrumented bolt, and an internally instrumented bolt. The internally instrumented bolt showed better stability and measurement accuracy. Two studies used a load cell in contact with a central rod within the specimen's bolt [22, 23].

Numerical analyses using the Finite Element Method (FEM) proposed in the literature for bolt-loaded specimens aim to calculate fracture parameters with simplified geometries [24, 15] or the stress field and distribution of diffusive hydrogen concentration around the crack tip [25]. Dadfarnia *et al*. [24] simulated a two-dimensional model of half the Modified-WOL specimen without the bolt and pin, adopting a crack propagation model coupled with a hydrogen diffusion model. Wei *et al*. [25] simulated half of a three-dimensional model of the Modified-WOL specimen, without the bolt and pin, to investigate the effect of corrosion points on the stress field and the distribution of diffusive hydrogen concentration. Sochu *et al*. [15] performed an experimental analysis and a three-dimensional FEM analysis of a Modified-WOL specimen, where they modeled all contact regions with friction using the Penalty method and used Quarter-Point elements at the crack tip. However, none of these approaches provide information on the mechanical behavior of the set: specimen, bolt and reaction pin.

Despite the importance of the Modified-WOL specimen, a consensus is lacking in the literature regarding the best location for sensor installation, potentially influencing its mechanical response. Based on that, this study aims to explore the mechanical behavior of the three components constituting the Modified-WOL specimen test by three-dimensional (3D) FEM simulations, contributing to the identification of regions of significant interest and, ultimately, the selection of the best location for strain gauge installation.

2 Theoretical foundation

2.1 Numerical Formulations for Mechanical Contact Problems

A mechanical contact problem can be analyzed as a mass-spring system [26]. A mass point m is suspended by a spring with stiffness k and has a rigid barrier that restricts its displacement u. The potential energy Π of this system is given by eq. (1), as derived by Konyukhov and Izi [26]. Structurally, eq. (1) represents the equilibrium equation, whose global minimum is the solution to this contact problem, and u represents the nodal displacements.

$$\Pi(u) = \frac{1}{2} k u^2 - m g u \rightarrow min \tag{1}$$

The non-penetration condition is expressed by the penetration function $p(u)$, given by the inequality in eq. (2), considering the total height H of the system and the length l of the undeformed spring [26]. Thus, the optimal solution that minimizes $\Pi(u) \rightarrow min$ of eq. (1) that is subjected to the constraint $p(u)$ of eq. (2) is sought.

$$p(u) \coloneqq l + u - H \leq 0 \tag{2}$$

To solve this mechanical contact problem, one of the methods of Lagrange Multipliers, Penalty, and Augmented Lagrangian can be used. These methods are already implemented in major FEM-based software, such as ANSYS®.

2.2 Augmented Lagrangian Method

The Augmented Lagrangian method, as presented by Konyukhov and Izi [26], offers an alternative to the

Lagrange Multipliers and Penalty methods for satisfying the non-penetration condition without the need for an additional variable, such as the Lagrange multiplier λ. This method is based on the formulation in eq. (3).

$$L(u) = \Pi(u) + \lambda\, p(u) + \frac{1}{2}\,\varepsilon\, p^2(u) \rightarrow min \tag{3}$$

In eq. (3), the functional *L(u)* combines terms from the Lagrange Multipliers and Penalty methods, depending only on the displacement *u*. An iterative procedure known as the Lagrange multiplier augmentation is used to calculate λ. Thereby, the Augmented Lagrangian method is less sensitive to the contact normal stiffness ε and converges to the exact non-penetration condition $p(u) = 0$ if the number of iterations tends to infinity [26]. In practice, the iterations continue until the obtained penetration is less than a pre-established tolerance.

3 Methodology

A homogeneous, isotropic, and linear elastic material model was adopted in this FEM simulation, using API 5CT P110 steel for the test specimen and 17-4 PH (H900) stainless steel for the bolt and pin. The material properties are presented in Tab. 1. Due to geometric asymmetry and its role in load transfer, the thread of the bolt and the specimen was considered. The geometries followed ISO 7539-6 standard [3], with the specimen thickness of 11 mm and fine metric threads. The Augmented Lagrangian method was used as the nonlinear formulation of the frictionless contacts. The boundary conditions of this 3D simulation, considering the initial preparation of the specimen prior to the EAC test, was applied in three loading steps and four substeps each following a loading rate of less than 100 MPa$\sqrt{m}$/min recommended by ASTM E1681-23ε1 standard [4], with specific translation restrictions as if using a vice (Fig. 1a). A mesh with 264,705 elements and 385,423 nodes was used (Fig. 1b), consisting of 10-node tetrahedral solid elements of the SOLID187 type, based on a convergence study of the results and the mesh quality.

Table 1. Mechanical properties of the steels adopted.

Steel	Elastic Modulus [Pa]	Poisson's Ratio	Yield Stress [Pa]	Ultimate Tensile Strength [Pa]	Rockwell C hardness	Reference
API 5CT P110	2.16×10^{11}	0.3	8.96×10^{8}	9.78×10^{8}	-	[27]
17-4 PH (H900)	2.16×10^{11}	0.3	1.17×10^{9}	1.31×10^{9}	40	[28]

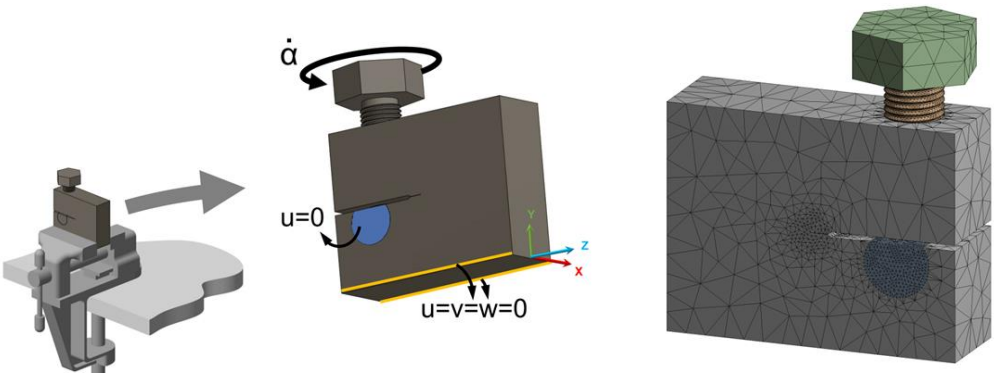

(a) (b)

Figure 1. (a) Boundary conditions and (b) mesh of the 3D simulation.

4 Results and Discussion

Unlike simplified geometry models used in the literature [15, 24, 25], our study incorporated the threads of the bolt and specimen, providing a more detailed view of the mechanical interactions and the regions of interest

for sensor installation. Fig. 2a shows the von-Mises stress field distribution in the assembly at the last simulation substep. Figures 2b and 2c detail the stress field in the reaction pin and bolt, respectively. Fig. 2a reveals that the maximum stress occurs at the crack front due to the stress singularity, characterized by the asymptotic increase in the stress field in this region [5]. Figure 2c shows the effect on the bolt thread due to interaction with the specimen, with greater engagement near the contact with the pin and higher stresses at the thread root on this part. The modeling adopted in this simulation was evaluated through comparisons between the numerical results obtained for the load applied by the bolt and the load calculated using the ISO 7539-6 [3] standard expression, resulting in average errors of 1.15% ± 0.31%.

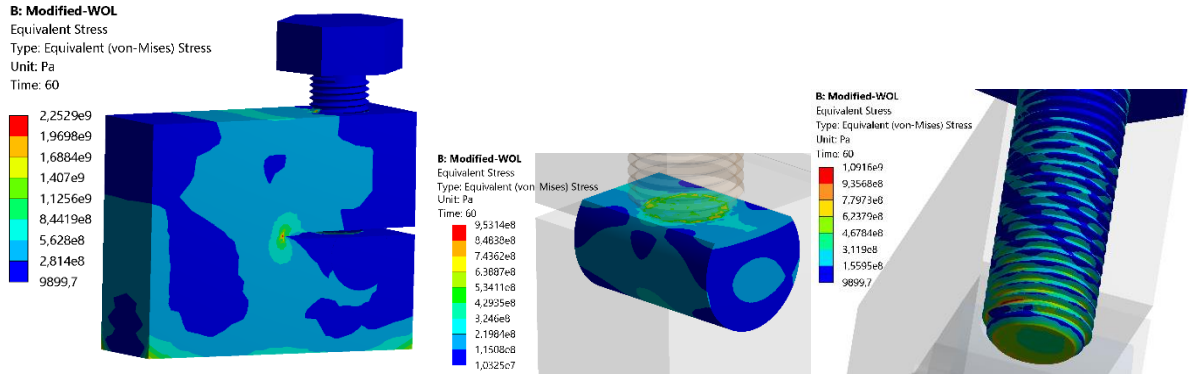

(a) (b) (c)

Figure 2. Von-Mises stress field distribution (a) in the assembly, (b) in the reaction pin, and (c) in the bolt.

Based on these results, we identified the following regions of interest for strain gauge installation, shown in Fig. 3: Region 1) inside the bolt, aligned with its axial axis; Region 2) at the top face of the specimen; Region 3) at the back face of the specimen; Region 4) inside the reaction pin, aligned with its middle plane. Installation in Region 1 represents an instrumented bolt [16-23]. Installation in Region 2 represents an adaptation of the ASTM E1820 [29] recommendation for C(T) specimens. Region 3 represents the BFS technique [14-15]. Region 4 adapts the approach of [7, 11].

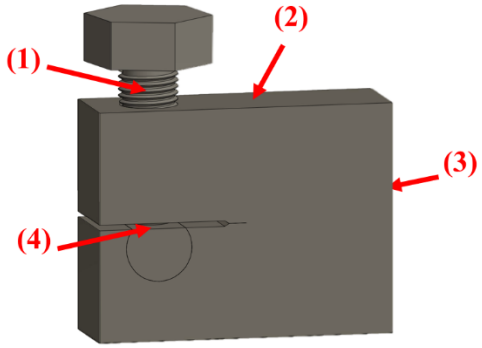

Figure 3. Regions of interest for strain gauge installation.

In these four regions, we evaluated the equivalent elastic strain variation along the paths shown in Fig. 4. Marker 1 shown from Fig. 4a to Fig. 4d indicates the start, and marker 2 indicates the end of each path. Figure 4 presents the results for the last simulation substep, but the other substeps were also evaluated.

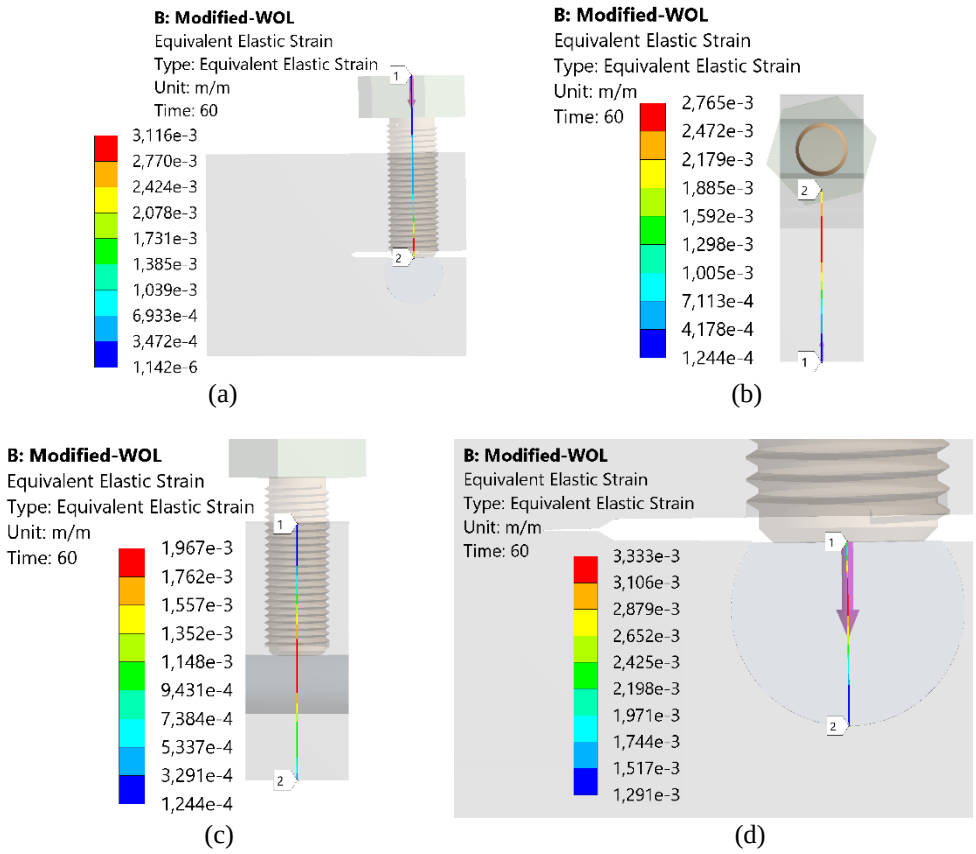

Figure 4. Elastic strain variation at the last substep along defined paths (a) in Region 1, (b) in Region 2, (c) in Region 3, and (d) in Region 4.

Figure 5 shows the 3D graphs of the strain variation in function of the relative position and the bolt load. The relative position means the distance along the path divided by its total length. The bolt load was obtained from each simulation substep at the contact region between the bolt and pin and was incremented in each substep. In Fig. 5a, the most significant strain field in Region 1 occurs near the contact with the reaction pin, peaking at a relative position of 0.94, i. e., 6% of the total bolt length from this contact point. Figure 5b shows Region 2 with a more distributed strain field, peaking at 0.75 relative position, which maximum value is lower than in Region 1. Figure 5c shows a distributed strain in Region 3, peaking at 0.54 relative position, with the maximum value lower than in Region 2. Figure 5d shows Region 4 with a uniform distribution along the analyzed path, with a higher maximum value than the other regions at 0.29 relative position.

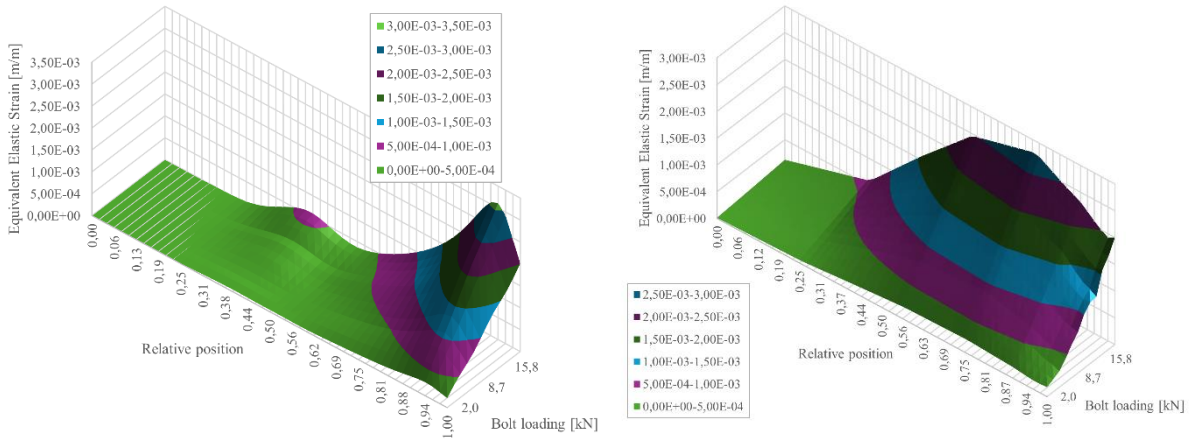

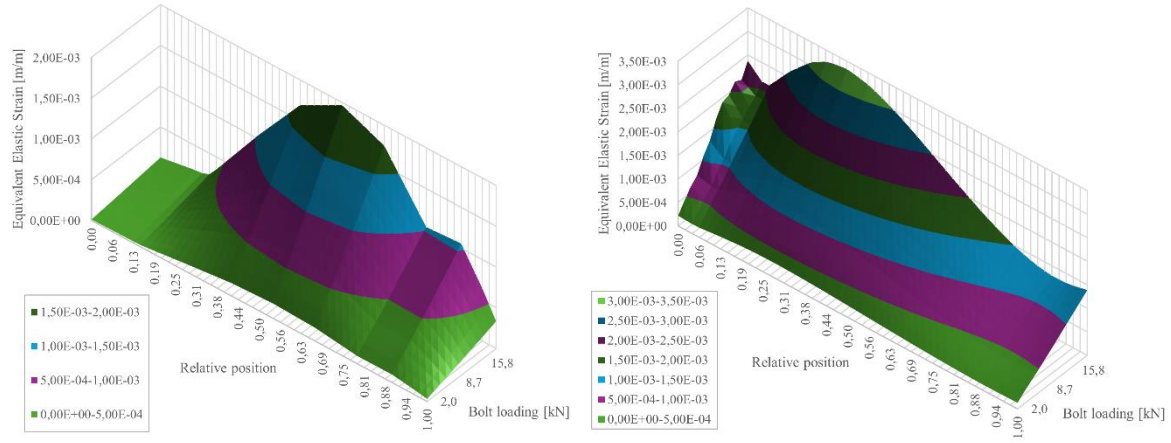

(c) (d)

Figure 5. Strain versus relative position versus bolt load for (a) Region 1, (b) Region 2, (c) Region 3, and (d) Region 4.

Based on these results and the EAC test characteristics, Regions 2 and 3, when in direct contact with the corrosive environment of the environmental chamber, could suffer corrosion, becoming more fragile and altering the mechanical behavior obtained from this simulation. Additionally, the corrosive environment could degrade the strain gauges as it happens to the clip gauge [4]. Region 4 would be an excellent choice for instrumentation, depending on the reaction pin dimensions. However, for the specimen geometry in this study, with a thickness of 11 mm and dimensional ratios recommended by [3], Region 4 becomes too small for strain gauge installation. Therefore, the best option is to instrument the bolt with a cylindrical strain gauge placed at a distance from the bolt base equivalent to 6% of the total bolt length. Thus, the strain gauge is protected from the chemical reactions with the environmental chamber and can be reused in multiple tests along with the bolt.

5 Conclusions

Given the lack of consensus in the literature regarding the best location for strain gauge installation in the Modified-WOL specimen, we simulated with FEM a 3D model of this specimen, assembled with the bolt and the reaction pin, considering the initial loading applied by the bolt during the specimen preparation stage, which is prior to the EAC test. In this modeling we incorporated the threads of the bolt and specimen, providing a more detailed view of the mechanical contact interactions The objective was to identify and evaluate regions of interest for the strain gauge installation. Based on the distribution of elastic strain along the paths in four different regions for each bolt loading, we selected the region inside the bolt, along its axial axis. This choice has direct implications for the practice of monitoring the initial bolt loading ate the preparation stage and during the EAC test, providing more accurate data and real-time measurements of the force transfer, the variation of K_I during the test, crack growth, and the threshold for K_{IEAC}.

Acknowledgements. This study was financed in part by the Coordenação de Aperfeiçoamento de Pessoal de Nível Superior – Brasil (CAPES) – Finance Code 001. The Postgraduate Program in Mechanical Engineering (PPGEM) and the Instituto de Pesquisa em Petróleo e Energia (i-LITPEG) from the Federal University of Pernambuco (UFPE, Brazil) also supported this work.

Authorship statement. The authors hereby confirm that they are the sole liable persons responsible for the authorship of this work, and that all material that has been herein included as part of the present paper is either the property (and authorship) of the authors, or has the permission of the owners to be included here.

References

[1] J. Toribio and A. M. Lancha, "Overload retardation effects on stress corrosion behaviour of prestressing steel". *Construction and Building Materials*, v. 10, n. 7, pp. 501-505, 1996.
[2] Y. P. Zhang *et al*., "Hydrogen-assisted cracking of T-250 maraging steel". *Materials Science and Engineering A*, v. 471, n. 1-2, pp. 34-37, 2007.
[3] ISO, "ISO 7539-6: Corrosion of metals and alloys — Stress corrosion testing — Part 6: Preparation and use of precracked specimens for tests under constant load or constant displacement". International Organization for Standardization, 2018.
[4] ASTM International, "ASTM E1681-23ε1: Standard Test Method for Determining Threshold Stress Intensity Factor for Environment-Assisted Cracking of Metallic Materials". ASTM International, 2024.
[5] T. L. Anderson, *Fracture Mechanics - Fundamentals and Applications*. Taylor & Francis Group, 2005.
[6] R. W. Hertzberg, R. P. Vinci and J. L. Hertzberg, *Deformation and Fracture Mechanics of Engineering Materials*. John Wiley & Sons Inc., 2012.
[7] K. A. Nibur *et al*., "Measurement and interpretation of threshold stress intensity factors for steels in high-pressure hydrogen gas". *Sandia Report*, Sandia National Laboratories, 2010.
[8] M. Cabrini *et al*., "Hydrogen embrittlement behavior of HSLA line pipe steel under cathodic protection". *Corrosion Reviews*, v. 29, pp. 261-274, 2011.
[9] Y. Ito *et al*. "Effect of hydrogen on crack growth behavior in F82H steel using small-size specimen". In: M. A. Sokolov and E. Lucon, *Small Specimen Test Techniques*, ASTM International, v. 6, pp. 209-224, 2015.
[10] L. Gu *et al*. "Measurement and Analysis of Hydrogen Distribution in Stress Environment Using Vickers Microhardness Technique". *Advances in Materials Science and Engineering*, v. 2018, pp. 1-8, 2018.
[11] B. P. Somerday and K. A. Nibur, "Effect of Applied K Level on the Crack-Arrest Threshold in Hydrogen Environments: Mechanics-Based Interpretation". *Corrosion*, v. 75, n. 8, pp. 929-937, 2019.
[12] D. Nie *et al*. "Stress corrosion cracking behaviors of FV520B stainless steel used in a failed compressor impeller". *Engineering Failure Analysis*, v. 116, 2020.
[13] Q. Ming *et al*. "Experimental Study on Stress Corrosion Crack Propagation Rate of FV520B in Carbon Dioxide and Hydrogen Sulfide Solution". *Results in Physics*, v. 6, pp. 365-372, 2016.
[14] T. Matsumoto *et al*. "Threshold stress intensity factor for hydrogen-assisted cracking of CR-MO steel used as stationary storage buffer of a hydrogen refueling station". *International Journal of Hydrogen Energy*, v. 42, pp. 7422-7428, 2017.
[15] W. Sochu *et al*. "Determination of Crack-Tip Opening Displacement in T-Type Wedge Opening Loaded Specimen". *Experimental Mechanics*, v. 60, n. 2, pp. 145-152, 2019.
[16] G. Vigilante, J. Underwood and D. Crayon, "Use of the Instrumented Bolt and Constant Displacement Bold-Loaded Specimen to Measure In-Situ Hydrogen Crack Growth in High-Strength Steels". *Fatigue and Fracture Mechanics*, v. 30, pp. 377–387, 2000.
[17] J. R. Scully and G. A. Young Jr., "The Effects of Temper, Test Temperature, and Alloyed Copper on the Hydrogen-Controlled Crack Growth Rate of an AI-Zn-Mg-(Cu) Alloy". In: *Corrosion2000*, NACE International, 2000.
[18] R. L. Sindelar *et al*. "Chloride-Induced Stress Corrosion Crack Growth Under Dry Salt Conditions: Application to Evaluate Growth Rates in Multipurpose Canisters". In: *ASME 2016 Pressure Vessels and Piping Conference*, ASME, 2016.
[19] A. J. Duncan *et al*. "Crack Growth Rate Testing With Instrumented Bolt-Load Compact Tension Specimens Under Chloride-Induced Stress Corrosion Cracking Conditions in Spent Nuclear Fuel Canisters". In: *ASME 2017 Pressure Vessels and Piping Conference*, ASME, 2017.
[20] L. Tjayadi, N. Kumar and K. L. Murty, "Accelerated crack growth experiments of SS304H for dry storage canister in substitute ocean water – Effect of temperature". *Materials Today Communications*, v. 23, 2020.
[21] P. C. Chung, G. Cragnolino and D. D. Macdonald, "Instrumented Loading Devices for Monitoring Environmentally Assisted Crack Growth in High Temperature Aqueous Systems". *Corrosion*, v. 41, n. 3, pp. 179-183, 1985.
[22] B. J. Buescher Jr. *et al*. "Load Apparatus and Method for Bolt loaded Compact Tension Test Specimen". US n. 5598738, 1997.
[23] G. Sui, E. A. Charles, and J. Congleton, "The effect of delta-ferrite content on the stress corrosion cracking of austenitic stainless steels in a sulphate solution". *Corrosion Science*, v. 38, n. 5, pp. 687-703, 1996.
[24] M. Dadfarnia *et al*. "On Modeling Hydrogen-Induced Crack Propagation Under Sustained Load". *The Minerals, Metals & Materials Society*, v. 66, n. 8, pp. 1390-1398, 2014.
[25] R. Wei *et al*. "Experimental study and numerical simulation on the SSCC in FV520B stainless steel exposed to H2S+Cl− Environment". *International Journal of Hydrogen Energy*, v. 43, n. 18, pp. 9059-9067, 2018.
[26] A. Konyukhov and R. Izi, "Introduction with a Spring-Mass Frictionless Contact System". In: A. Konyukhov and R. Izi. *Introduction to Computational Contact Mechanics - A Geometrical Approach*, Wiley, pp. 3-12, 2015.
[27] J. R. P. Corrêa *et al*. "Structural integrity assessment of a 5CT P110 steel riser pipe according to BS 7910:2013 standard". *International Journal of Pressure Vessels and Piping*, v. 188, pp. 1–8, 2020.
[28] ASTM International, "ASTM A564/A564M: Standard Specification for Hot-Rolled and Cold-Finished Age-Hardening Stainless Steel Bars and Shapes.". ASTM International, 2019.
[29] ASTM International, "E1820-13: Standard Test Method for Measurement of Fracture Toughness". ASTM International, 2015.